ATION PAGE

Form Approved
OBM No. 0704-0188

1 hour per response, including the time for reviewing instructions, searching existing data sources, gathering and nation. Send comments regarding this burden or any other aspect of this collection of information, including suggestions Information Operations and Reports, 1215 Jefferson Davis Highway, Suite 1204, Arlington, VA 22202-4302, and to 88), Washington, DC 20503.

1. Agency Use Only *(Leave blank).*

2. Report Date. February 1994

3. Report Type and Dates Covered. Final - Journal Article

4. Title and Subtitle.
Laboratory Comparisons of Acoustic and Optical Sensors for Microbubble Measurement

5. Funding Numbers.
Program Element No. 0601153N
Project No. 03204
Task No. 040
Accession No. DN250048
Work Unit No. 13312Q, 13311Q

6. Author(s).
Ming Yang Su, Douglas Todoroff*, and John Cartmill**

7. Performing Organization Name(s) and Address(es).
Naval Research Laboratory
Ocean Sciences Branch
Stennis Space Center, MS 39529-5004

8. Performing Organization Report Number.
JA331:086:92

9. Sponsoring/Monitoring Agency Name(s) and Address(es).
Office of Naval Research
800 N. Quincy Street
Arlington, VA 22217

10. Sponsoring/Monitoring Agency Report Number.
JA 331:086:92

11. Supplementary Notes.
Published in JAOT.
*Coastal Systems Station, Dahlgren Division, Panama City, FL
**Planning Systems Inc., Slidell LA

12a. Distribution/Availability Statement.
Approved for public release; distribution is unlimited.

13. Abstract *(Maximum 200 words).*

This paper presents the results of a recent comparison between three microbubble size spectrum measurement systems. These systems are the light-scattering bubble counter, the photographic bubble-imaging system, and the acoustic resonator array. Good agreement was formed among these three systems over the bubble size range appropriate for each system.

14. Subject Terms.
Microbubbles, wave breaking

15. Number of Pages. 12

16. Price Code.

17. Security Classification of Report.	18. Security Classification of This Page.	19. Security Classification of Abstract.	20. Limitation of Abstract.
Unclassified	Unclassified	Unclassified	SAR

Reprinted from JOURNAL OF ATMOSPHERIC AND OCEANIC TECHNOLOGY, Vol. 11, No. 1, February 1994
American Meteorological Society

Laboratory Comparisons of Acoustic and Optical Sensors for Microbubble Measurement

MING YANG SU

Naval Research Laboratory Detachment, Stennis Space Center, Mississippi

DOUGLAS TODOROFF

Coastal Systems Station, Dahlgren Division, Panama City, Florida

JOHN CARTMILL

Planning Systems Inc., Slidell, Louisiana

(Manuscript received 17 August 1992, in final form 25 May 1993)

ABSTRACT

This paper presents the results of a recent comparison between three microbubble size spectrum measurement systems. These systems are the light-scattering bubble counter, the photographic bubble-imaging system, and the acoustic resonator array. Good agreement was formed among these three systems over the bubble size range appropriate for each system.

1. Introduction

In the past decade, the importance of microbubbles to many physical, chemical, and biological phenomena in the near-surface air–sea boundary layers, both above and below the sea surface, has been well recognized and documented (Wu 1987). It is becoming increasingly certain that bubble plumes generated by ocean wave breaking play a significant role in underwater acoustic propagation and scattering problems. The effects of bubbles are seen in both high (10–400 kHz) and low (50–1000 Hz) frequency ranges through either single-bubble resonance or collected plume resonance (Prosperetti 1988; Henyey 1990).

Unfortunately, up to now no single ideal technique has been developed to measure microbubbles in either the laboratory or in the ocean. An ideal system would provide an adequate size range, a large sampling volume, a large spatial area and depth coverage, and quick response time, and be amenable for automatic data analyses. The need for such a bubble sensor system is clear, and it is still beyond our reach. At the present time, a combination of several different types of bubble sensors working in concert may give an overall acceptable performance.

The Coastal Systems Station (CSS), since 1984, and Naval Research Laboratory (NRL), since 1986, have been involved in the development of sensor systems for microbubble measurements in the field. The system developed by CSS is the light-scattering bubble counter (LSBC), and the two systems developed by NRL are the acoustic resonator array (ARA) and the photographic bubble-imaging system (PBIS). All three systems have been deployed independently to measure wave-generated bubbles in the sea, and they have been used in laboratory tanks for testing and calibration using artificially generated bubbles.

It is instructive to compare the performance of these three bubble sensor systems, which operate on entirely different optical and acoustic principles, under identical laboratory conditions. In 1990, CSS and NRL jointly carried out such a comparison test at CSS in Panama City, Florida. The purpose of this paper is to present the experimental results of this comparison test.

In section 2, the operation principles of CSS's and NRL's bubble sensors will be presented. In section 3, the methods for the comparison test will be described with the results presented in section 4. Finally, a summary and concluding remarks about these comparison tests on bubble measurement techniques will be made.

2. Operation principles of bubble sensors

We shall describe first, in detail, the operating principles of the three CSS and NRL bubble systems, which are involved in the laboratory comparison test. The five factors or criteria we shall use as a base for evaluating all the bubble sensors are

Corresponding author address: Dr. Ming Yang Su, Naval Research Laboratory, Stennis Space Center, MS 39529-5004.

F1—bubble size range (radius in microns),
F2—sampling volume,
F3—spatial coverage,
F4—sampling time, and
F5—data analysis complexity.

Here, the sampling volume (F2) refers to the instantaneous spatial volume sampled by the sensor, while the spatial coverage (F3) refers to the distance from the sensor location that can be measured by the sensor remotely. The sampling time (F4) is the appropriate time period required for obtaining a statistically reliable bubble density measurement; thus, it is related to (F2) and (F3). The data analysis complexity (F5) is whether or not a bubble measurements system is amenable to automatic processing of raw data to yield the bubble density.

a. Light-scattering bubble counter

The light-scattering bubble counter (LSBC) was originally designed and developed by C. S. Ling, Catholic University of America, for laboratory investigations of microbubbles upon the inception of cavitation in 1982 (Ling and Pao 1988). It has been further modified into a field system under CSS sponsorship. In addition to laboratory experiments and tests, this field system has been employed a few times in sea operations (Ling and Pao 1988; Su et al. 1988) in conditions ranging from fairly calm seas in the Gulf of Mexico to violent seas in the North Sea. Currently, this system is operated by CSS personnel.

This LSBC system is based on dark-field specular reflection for detection of microbubbles, and this principle is depicted in Fig. 1 [from Fig. 3 in Ling and Pao (1988)]. White light is critically reflected by the gas–water interface of a bubble that passes through a sampling volume A_1 of 5 mm × 6 mm × 0.4 mm = 0.012 cm^3 located within the center of an open-ended cylinder about 3.8 cm in diameter. The flow containing bubbles is sucked through this cylindrical cavity by a pump. The reflected light intensity is received by a photomultiplier detector, at an angle of 125° with respect to the incident light and is proportional to the square of the bubble radius. The coefficient of proportionality can be determined by the well-known relationship between the bubble size and its terminal velocity in a freely rising situation. This terminal velocity determination, during the sensor calibration, is facilitated by the second sampling volume A_2, which is parallel to A_1 and separated by a known distance (0.5 cm). The simultaneous recording of two light intensity signals from the two photomultipliers are correlated to provide the travel time over the separation distance.

For better signal-to-noise ratio, the square root of the photomultiplier voltage output is taken prior to being input to either an FM recorder with a 20-kHz bandwidth or a digital recorder after A/D (analog to digital) conversion at a rate of 20 kHz. Because of this operation on the data stream, the recorded signal is directly proportional to the bubble radius. Ling and Pao's (1988) Fig. 7 gives a calibration curve for the LSBC, showing that the sensor is linear from a radius

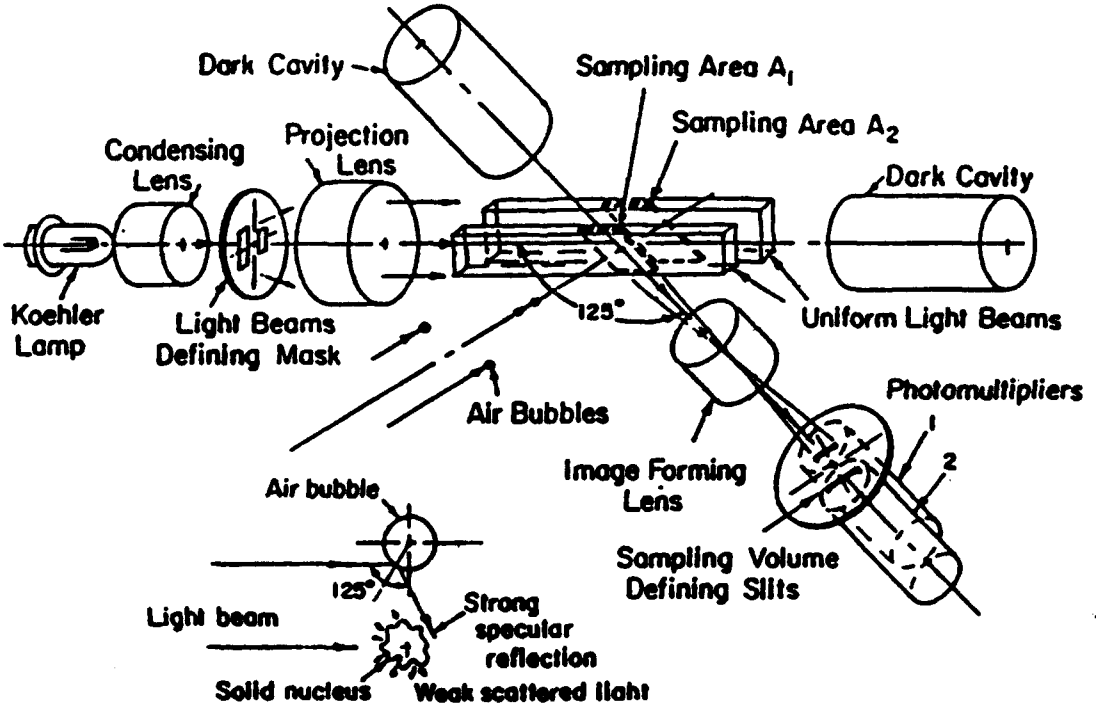

FIG. 1. A sketch of detection of microbubbles by dark field specular reflection used by the LSBC.

of about 10 μm to about 150 μm. In other calibrations, the sensor is shown to be useful for radius r up to 200 μm. The upper bound of r = 200 μm is due to the thickness of the sampling volume, 0.4 mm = 400 μm. In principle, this thickness can be increased, at the expense of lowering the maximum bubble density, since the sensor is allowed to have only one bubble present in the sampling volume at any given time, otherwise causing an erroneous reading. The LSBC can only be used in an in situ mode, and its sampling time is long, 10 min or more, due to its small sampling volume (0.012 cm^3). The technique is suited for automatic data analyses. With a mean flow velocity within the sampling volume of 0.5 m s^{-1}, the effective sampling volume per 10 min is a 5 mm × 6 mm × 0.5 m s^{-1} × 60 s × 10 min = 9000 cm^3.

b. Photographic bubble image system (PBIS)

The photographic bubble imaging system developed by NRL consists of a 35 mm camera in a waterproof housing and three underwater strobes mounted on a square stainless steel frame, as shown in Fig. 2. The three strobes (Ikelite) form an equilateral triangle with each side 43 cm. The strobes are located 14 cm behind the focal plane of the camera. This design principle follows essentially that of Johnson and Cooke (1979).

The camera system consists of the following components:

1) a Nikon F-3 camera body,
2) a Nikon 55-mm f/2.8 macro lens,
3) a Nikon MD-4 motor drive
4) a Nikon MF-4 250 exposure magazine, and
5) a Nikon MF-17 data back.

The lens is set for a magnification of 1:3, with an f-stop of f/11. The focal plane is located 34 cm from the film plane when the system is submerged, as shown in Fig. 3.

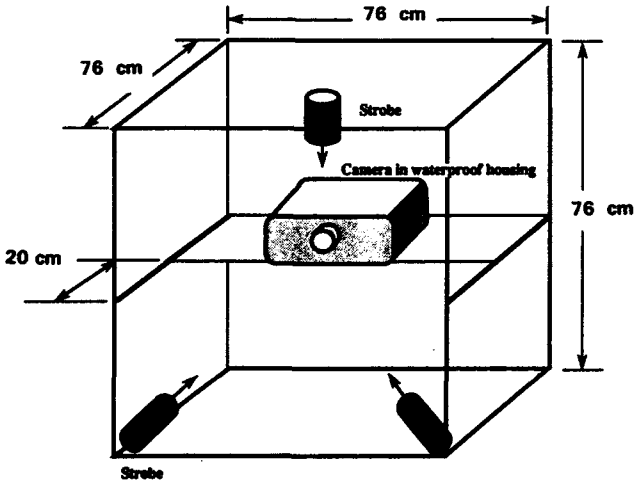

FIG. 2. PBIS configuration used in the comparison tests.

To determine the bubble size distribution, each photographic frame is viewed under a microscope. The Bausch and Lomb microscope used in the data analysis has a 10× objective and a 10× eyepiece for a total magnification of 100×. For bubble sizing, a calibrated 500-μm reticle with 10-μm divisions is used. An X–Y scale (1 mm × 1 mm) was fabricated to locate the position of each bubble in the frame. The bubbles produce a triangular pattern of dots that are specular reflections from the strobes. Each side of the triangle is measured to within 5 μm and recorded. These three lengths are then averaged and multiplied by a factor of 2.25 to obtain the bubble radius. The factor of 2.25 is needed to correct for the 1:3 image reduction and other geometric conversions. Figure 4 illustrates the measurement procedure.

Since the depth of field is proportional to the bubble size, then

$$\text{depth of field (m)} = 0.22 \times 0.022 \times \text{radius } (\mu\text{m}), \quad (1)$$

with aperture at f/11. The bubble density for each bubble size is computed first. The total bubble density is then obtained by summing up the individual bubble densities. These densities are then averaged over a 20-μm "bandwidth."

Based on the above relationship, the sampling volume per frame for r = 100 μm is about 10 cm × 15 cm × 2.2 cm = 330 cm^3, which is 27 500 times larger than that of the LSBC. Since the strobes have a charge time of about 5 s (allowing 12 photographs per minute), the equivalent total sampling volume per 10-min period is 330 × (60 × 10)/5 = 39 600 cm^3. This is about four times larger than the LSBC.

The photographic system has to be operated in situ, and its sampling time is about 2.5 min, which is equivalent to about 25 photographic frames. The bubble size range for this system is 50–500 μm in radius. The lower limit is caused by the intrinsic difficulty in discerning smaller bubbles on a photographic negative, even under a microscope, based both on our own experience and that of Walsh and Mulhearn (1987). On the other hand, the upper limit is due to the statistically high uncertainty associated with the slight probability of encountering bubbles larger than this radius in a limited number of photographic frames.

The most serious drawback of the photographic system, however, is related to the tedious analyses of the photographic negatives. The methods used by Johnson and Cooke (1979), Walsh and Mulhearn (1987), and our efforts presented here are all manual. An automatic pattern recognition scheme can certainly be developed for a digitized film, but this process is still cumbersome due to the great amount of digital data per frame. At present, we regard the photographic system as practical only for calibrating other bubble systems in laboratory, in the bubble radius range of its applicability. For this

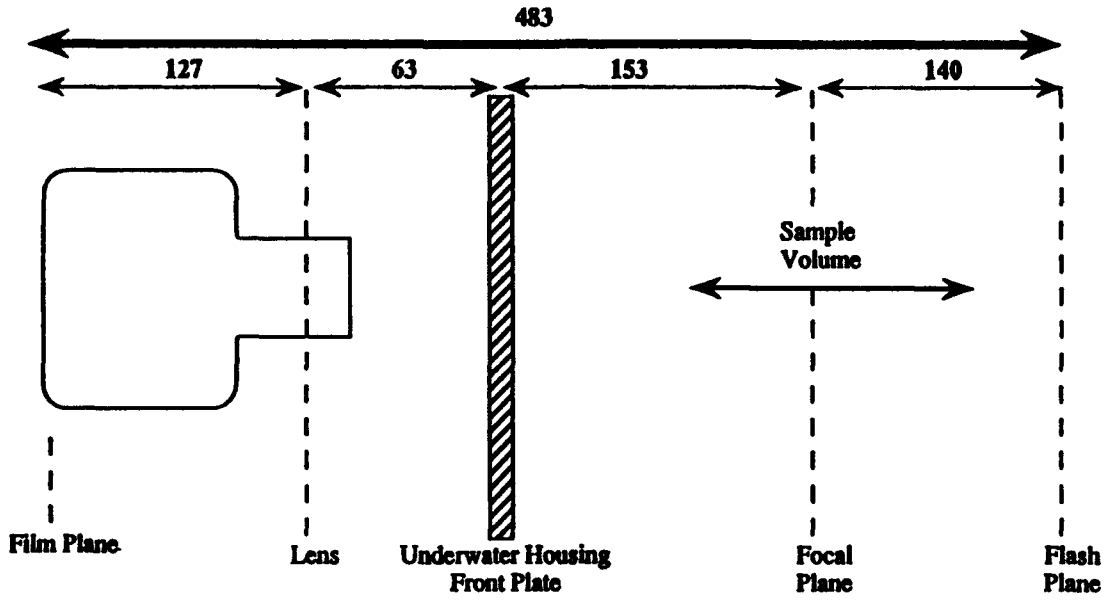

FIG. 3. Distance in millimeters between the camera, focal plane, and flashes. Not to scale.

special purpose, we can afford to do a very limited amount of manual processing, but we definitely do not recommend this system for routine field operations.

c. Acoustic resonator array (ARA)

The acoustic resonator array was constructed by NRL and is based on a design originally developed by Herman Medwin and his colleague of the Naval Postgraduate School (Medwin and Breitz 1989; Breitz and Medwin 1989). The system consists of a capacitive transducer plate and a reflector plate held in a parallel configuration. The transducer consists of a 0.5-mil sheet of aluminized mylar stretched (not glued) over an aluminum disk 26 cm in diameter. The aluminum disk is embedded in a 2.5-cm-thick disk of PVC and on the front of the mylar is a 2-mm coating of Eccothane, which forms a waterproof seal. The reflector plate consists of a stainless steel disk 6 mm thick mounted on PVC. A ceramic disk hydrophone, also coated with Eccothane, is embedded in the surface of the reflector plate. The transducer and reflector are separated by a distance of 24.1 cm. Figures 5 and 6 illustrate the construction of the resonator.

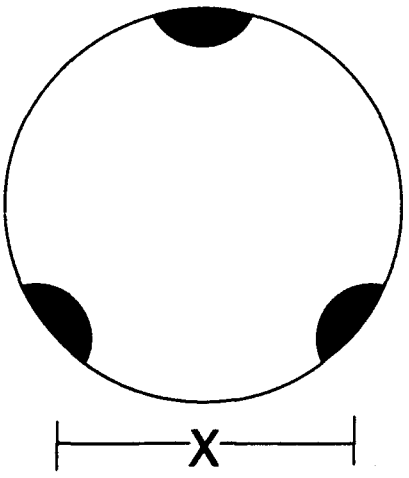

FIG. 4. Microbubble showing reflection of substrobes.

The operating principle of the acoustic resonator is based on two kinds of resonances: the first is the geometrical cavity resonance induced by the open space between the transducer and the reflector, which are parallel to each other. When a white noise is produced by the source transducer and reflected partially back and forth between these two plates, a series of standing acoustic waves are created within this open cavity between the two plates. For a separation of 24.1 cm between the two plates currently used in our bubble sensor, the fundamental frequency of the standing waves is close to 3 kHz and 32 higher harmonics also appear in the 100-kHz bandwidth of the white noise. The second type of resonance is individual bubble resonance due to excitation by acoustic waves, which has an equivalent cross section about a thousand times larger than the corresponding geometrical cross section of a bubble. For the fundamental frequency of 3 kHz, the resonant bubble radius is about 1200 μm, while for the highest harmonic frequency of 99 kHz, the resonant bubble radius is about 34 μm.

If we were to use a 400-kHz bandwidth white noise instead of the 100 kHz currently used, then the lower limit of the bubble size would be reduced to about 8.5 μm. However, for a frequency much higher than 100 kHz, the acoustic extinction (which includes both acoustic scattering and absorption) is no longer mainly

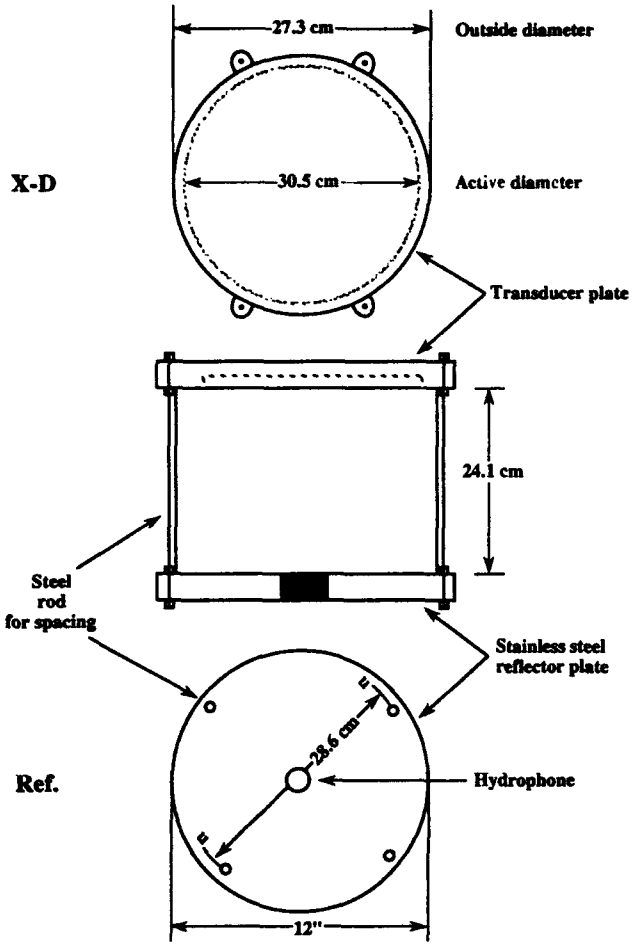

FIG. 5. Schematic diagram of NRL's acoustic resonator.

from the individual bubble resonance, but is also from the off-resonance acoustic extinction of larger bubbles. A much more sophisticated inversion scheme such as those recently presented by Commander and McDonald (1991) would then be needed. On the other hand, if the separation between the two plates is doubled, then the upper limit of the bubble radius will be doubled as well, to a value of 2.4 mm. The price to pay for extending the range to this larger bubble radius is a poorer geometric resonance between the two plates. With the above two possible adjustments and improvements, the acoustic resonator is believed to be capable of measuring bubbles with radii from about 8 μm to 2.5 mm.

The complete block diagram of the system, shown in Fig. 7, was constructed and integrated by NRL for use at sea. The transducer is connected to a 300-V dc polarizing battery and amplified white noise. The white noise is produced from the output section of an HP-3561A dynamic analyzer and is amplified by an Instruments Incorporated Model L2 power amplifier. The signal received by the hydrophone is fed into an Ithaco Model 143E preamplifier that provides 20 dB of gain and matches the high impedance of the hydrophone to the low impedance of the transmission cable. The signal is then input into the HP-3561A dynamic analyzer where its power spectrum is calculated by the fast Fourier transform (FFT) and then averaged. The measurement time is about equally divided for data acquisition and for FFT computation (Fig. 8). After 100 FFTs are averaged, which takes about 10 s, the dataset is then downloaded to an HP-9836 or other computer where it is stored.

The conversion of the acoustic resonator data to bubble size distribution is based on the formula (Breitz and Medwin 1989)

$$\eta_0(a) = \frac{2\pi\Delta f}{c\sigma 10^6 \delta a}, \tag{2}$$

where η_0 is the zeroth-order bubble density, c is the speed of sound in water, σ is the extinction cross section at resonance, Δf is the increase in resonance width, δ is the damping constant at resonance, and a is the bubble radius.

The differences in resonance heights between the FFT's with bubbles present and with a bubble-free reference case (Fig. 9) is then used to compute the Δf used in Eq. (2). For more details, see Breitz and Medwin (1989). An initial bubble distribution η_0 is then computed for each case. A correction for the contribution of off-resonance bubbles is then computed by integrating the equation

$$\alpha_B(f) = -4.3 \int_{a_1}^{a_2} \sigma\eta(a)da, \tag{3}$$

where $a_1 = 34$ μm and $a_2 = 1200$ μm. With $\eta(a)$ replaced by $\eta_0(a)$ and then substituting into

$$\eta(a_\eta) = \eta_0(a_\eta)\left[\frac{\alpha_B(f_\eta)}{\alpha(f_\eta)}\right]. \tag{4}$$

This produces the modified and corrected first-order bubble distribution, $\eta_1(a)$. This last correction can be carried to a higher order, if desired, by repeating the above procedure.

The bubble radius range for the current NRL's acoustic resonator array is 34–1200 μm, with a scattering volume about 1250 cm^3 as determined experimentally by Breitz and Medwin (1989). Assuming that the ARA near the sea surface is under the action of orbital motion of ocean waves with 2 m in wave height and 5 s in wave period, and further assuming that the mean flow rate passing through the resonator is about one-quarter of the maximum orbital velocity, the total scattering volume over a 10-min period is about 6 $\times$ 10^6 cm^3, which is about 600 times larger than the LSBC and 150 times larger than the PBIS. The ARA is an in situ sensor, has a fast response time of 10 s or less for a reliable measurement of the bubble density, and is amenable to fast automatic data processing.

At the present configuration, the NRL's ARA is op-

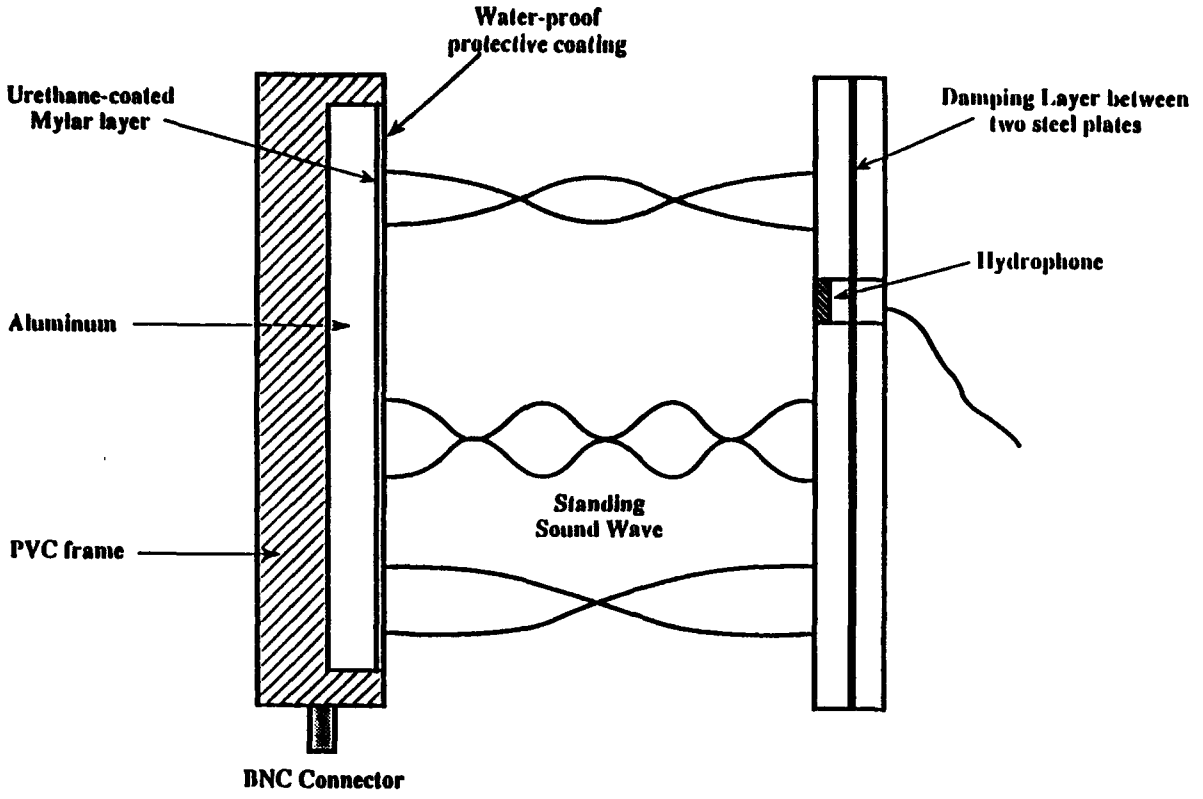

FIG. 6. Construction details of NRL's acoustic resonator.

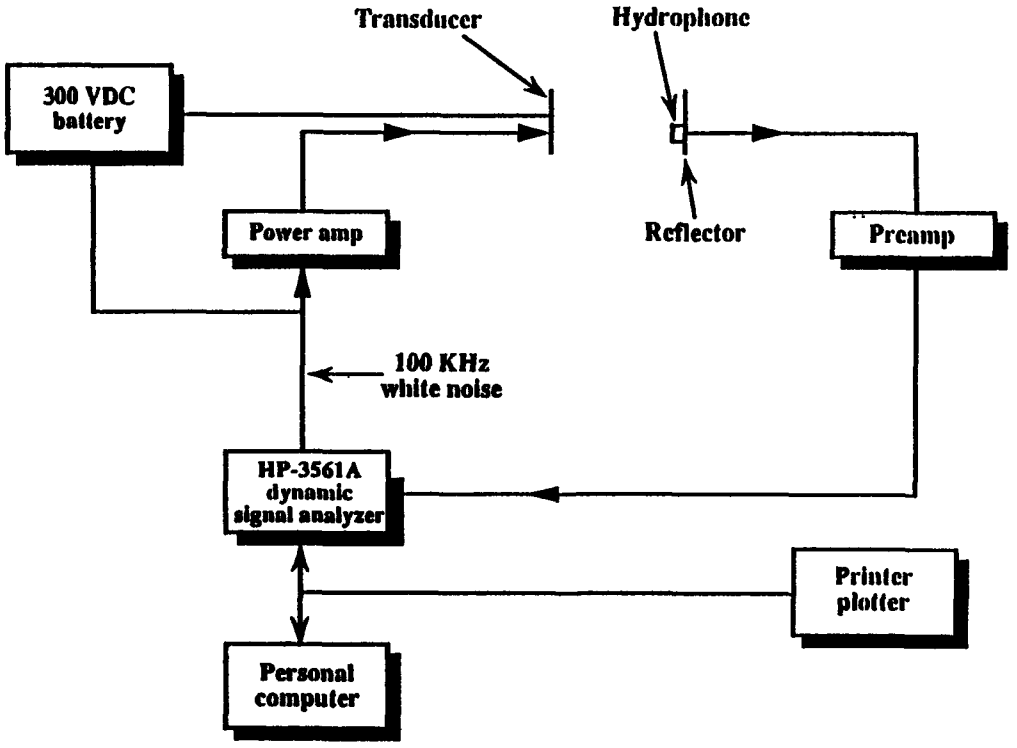

FIG. 7. Block diagram of acoustic resonator system.

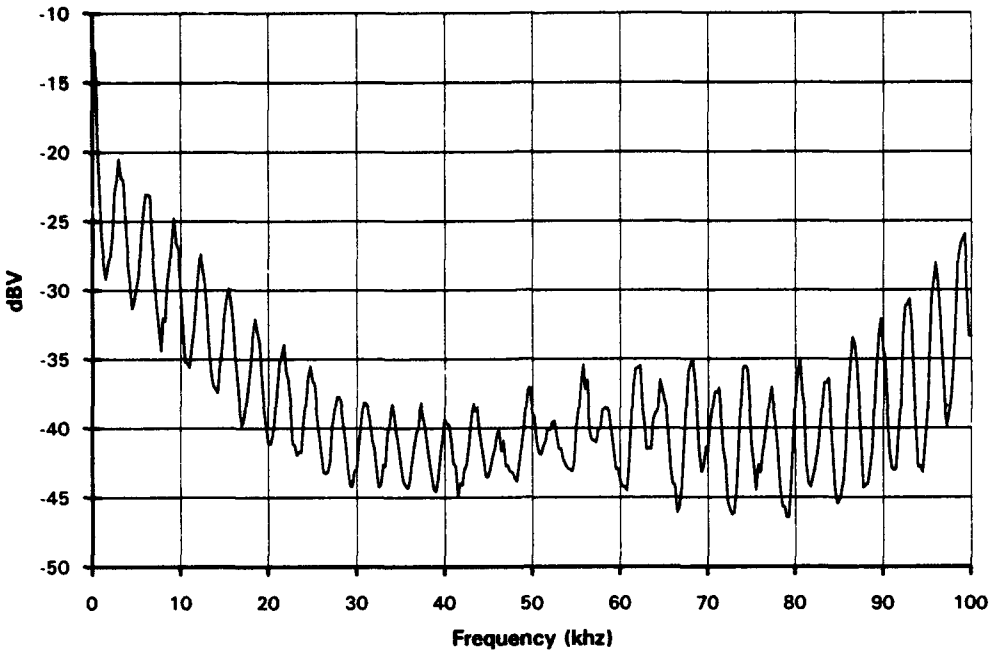

FIG. 8. Sample reference (bubble-free) curve from the acoustic resonator 0–100 kHz.

erated in the field by being tethered to a research vessel by a cable about 150 m long. But the system can be easily converted into an autonomous system with battery power for about 100 h of continuous operation.

3. Comparison tests

The comparison tests among the CSS's LSBC and NRL's PBIS and ARA were conducted at CSS, Panama City, using two freshwater test tanks in 1990.

The first test was between ARA and PBIS and the second test was between ARA and LSBC. In both tests, we employed three methods for generating bubble plumes (see Figs. 10a–c). The first method (Fig. 10a) used electrolysis with the bubble-producing wire wrapped around a 30-cm-long rod that was made to sweep over 80° to generate wider and more homogeneous bubble plumes. The second method produced bubbles by using a series of 15 hypodermic needles

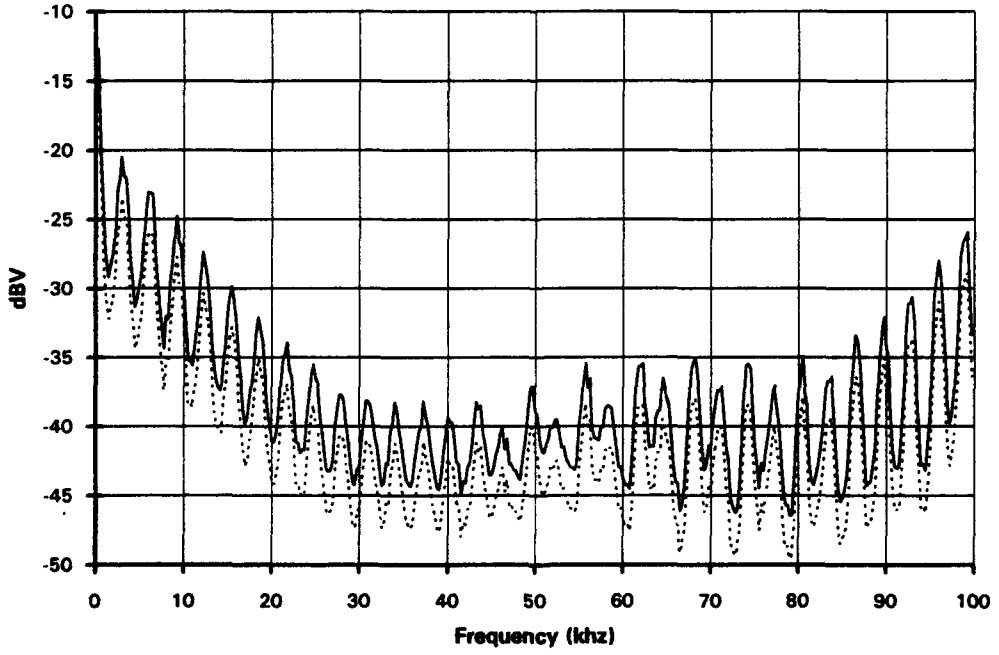

FIG. 9. Sample reference and bubble curve from the acoustic resonator 0–200 kHz.

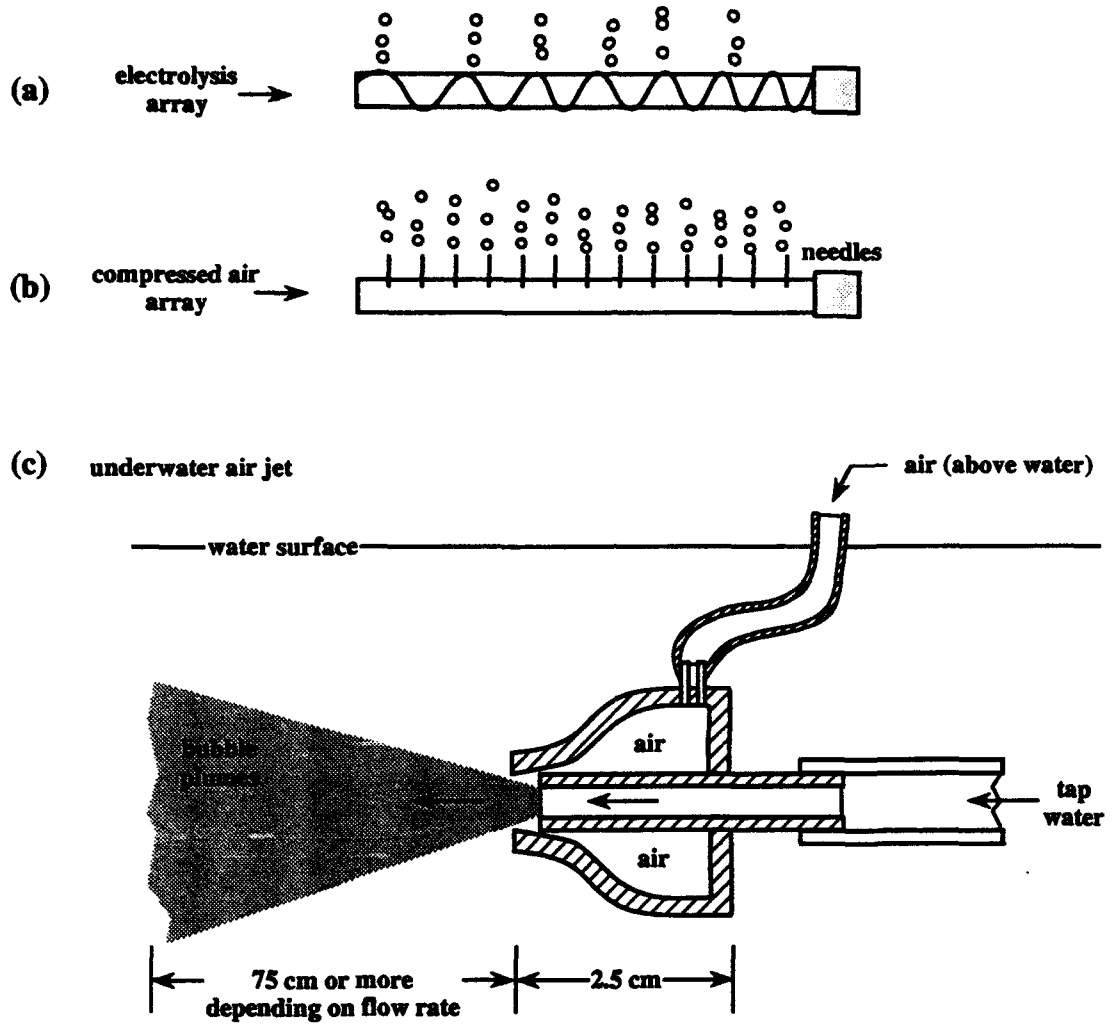

FIG. 10. Three methods employed for bubble generation: (a) electrolysis wire wrapped on a sweeping rod, (b) compressed air passed through needles on a sweeping tube, and (c) underwater jet air entrainment.

mounted on a copper tube, which is connected to a compressed air tank (Fig. 10b). This tube assembly also sweeps in the same way as the first method. The third method used an underwater jet for entraining air into the water in such a way (Fig. 10c) that a large bubble plume is created. The bubble size range created by the underwater jet is wide, from tens of microns to several millimeters. The bubble density may be controlled to a certain degree by varying the flow rate of the input tap water and by adjusting the jet head location and direction relative to the sampling volume of bubble sensors.

After analyzing and comparing of the bubble densities measured by these three bubble sensor systems using these three different methods for providing bubble plumes, we found that the third method of underwater jet is the most satisfactory for providing more continuous bubble density over the range from 30 to 1200 μm than the first two methods. For this reason, all the discussions on bubble tests shall be restricted to those being employed by the underwater jet only.

During the first comparison test between ARA and PBIS, the two systems were hung from two supporting beams on the top of the test tank, with PBIS placed above the ARA, as shown in Fig. 11. A bubble plume was generated about 65 cm below the ARA. Thus, the same bubble plume rose through the sampling volumes of the two bubble sensors that were centered about 3.0 and 3.4 m, respectively, below the water surface. Data were collected simultaneously by both sensors under this condition during the test.

During the second comparison test between LSBC and ARA, again both sensors were hung in the water tank, as shown in Fig. 12, in such a way that the flow intake opening of the LSBC was located about 5 cm above the top edge of the ARA. Again, the same bubble plumes passed through the sampling volumes of the two bubble detectors that were centered about 1.6 and

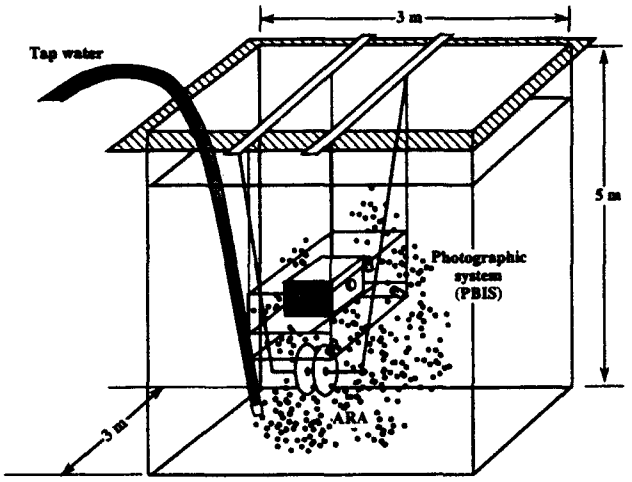

FIG. 11. Configuration of NRL's ARA and PBIS used in comparison test.

1.95 m, respectively, below the water surface. The water in the entire test tank was made to be fully saturated with air prior to the test so that the effects of natural degasing of air bubbles into the surrounding water was minimized during their free rise from the first sampling volume at the bottom to the second sampling volume at the top. The pressure differential effect on the bubble size is very small (about 1.5% of the bubble radius) because the separation between the two scattering volumes is only about 35 cm.

Since, in both series of comparison tests, the centers of the two scattering volumes of the pair of bubble sensors were at different water depths, any single bubble will change its radius traveling from one volume to the next. The ambient pressure effects on bubble size have been corrected.

Each of the two comparison tests were repeated ten times by the first and second methods, and five times with varying bubble densities by the third method of bubble generation.

The test data collected were processed according to the principles and formula as described in section 2 and finally expressed in the bubble density in number of bubbles per cubic meter per micron range of the bubble radius versus bubble radius in the customary log–log plot for accommodating the large dynamic range of the density over a radius range of 10–1000 μm.

4. Results of the comparison tests

We shall present first results of the test between the acoustic resonator array (ARA) and the photographic bubble imaging system (PBIS). Figures 13, 14, and 15 are three (out of five) cases of this comparison. The other two cases show similar results. In each plot we show the bubble densities measured by the two systems under the same conditions. Overall good agreement between these two bubble densities over the radius range of 80–400 μm is observed. The larger fluctuation seen in the bubble density by the PBIS is believed to be due to an insufficient number of photographic frames taken and analyzed, that is, statistical fluctuation due to undersampling. Furthermore, the bubble densities at radii less than 80 μm is somewhat lower for PBIS. This is attributed to the reduced sampling volume, caused by the smaller depth of field, and to the relative insensitivity of the film for smaller bubbles (Walsh and Mulhearn 1987). On the other end of the bubble radius range, the bubble density by the PBIS is also lower than that by the ARA. This might be also caused by statistical undersampling, since there are only a few large bubbles in the frames.

Figure 16 shows three successive bubble densities each averaged over 10 min by the ARA using the underwater jet for bubble generations. Very good consistency among them is observed over the radius range from 34 to 600 μm. This clearly shows the steadiness of the bubble plume generation.

Next, we present the results of comparison tests between the ARA and the light-scattering bubble counter

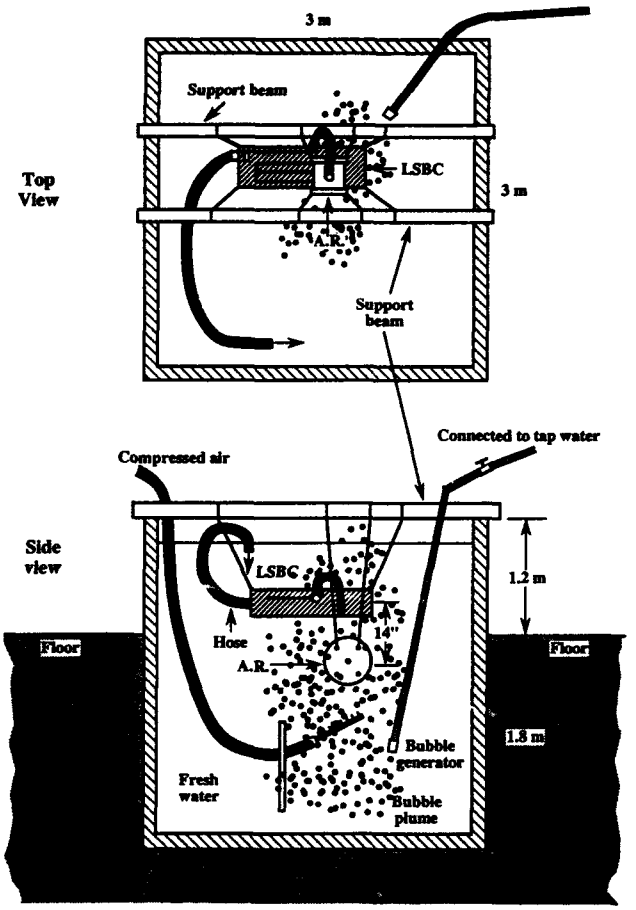

FIG. 12. Configuration of ARA and LSBC used in comparison test.

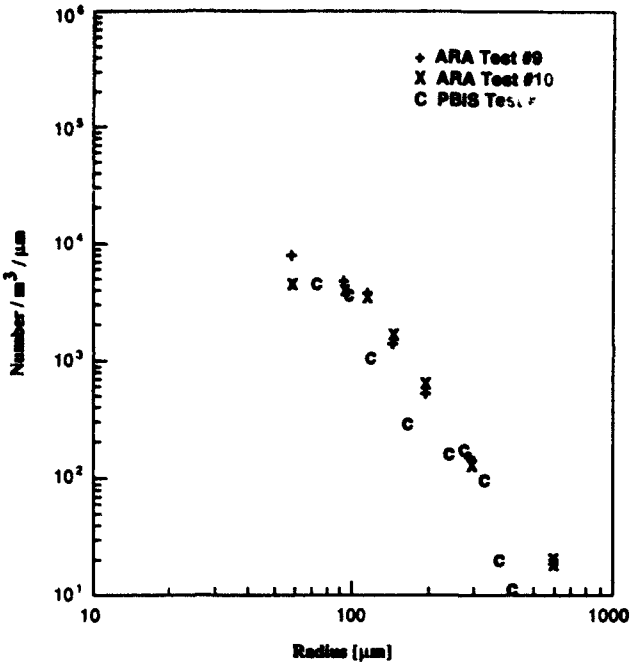

FIG. 13. Comparison of bubble densities measured by PBIS and ARA.

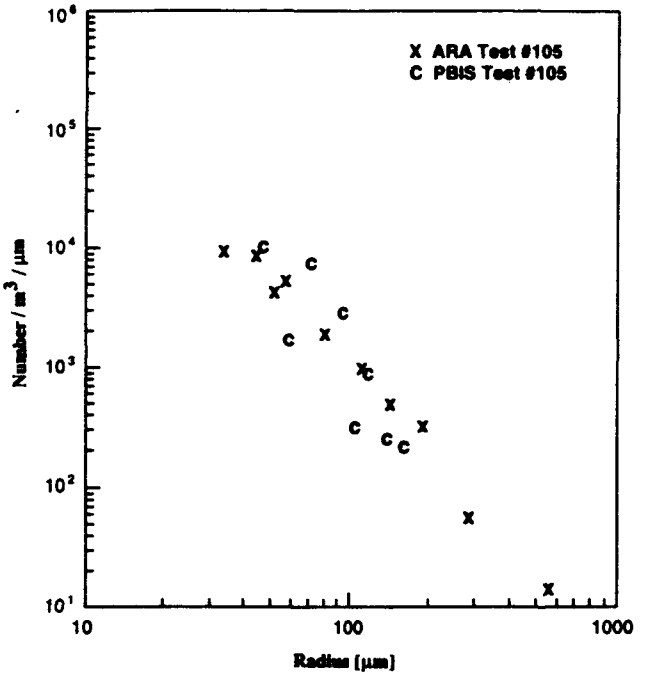

FIG. 15. Comparison of bubble densities measured by PBIS and ARA.

(LSBC). Three (out of five) bubble densities obtained by the two different sensors using three variations in flow rates of the underwater jet are shown in Figs. 17, 18, and 19. The other two cases show similar results. One can see clearly from these figures that the bubble densities obtained by these two methods agree remarkably well in the radius range of 34–200 μm, which is currently the applicable radius range of the LSBC, while the applicable range of ARA extends to 1200 μm.

Among the three bubble sensors compared—that is, ARA, LSBC and PBIS—we have reasons to think that the LSBC is the most accurate sensor in the bubble

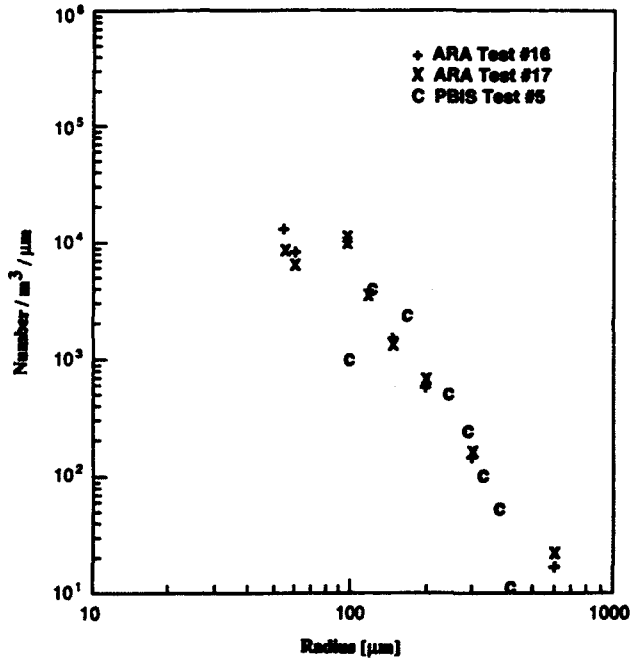

FIG. 14. Comparison of bubble densities measured by PBIS and ARA.

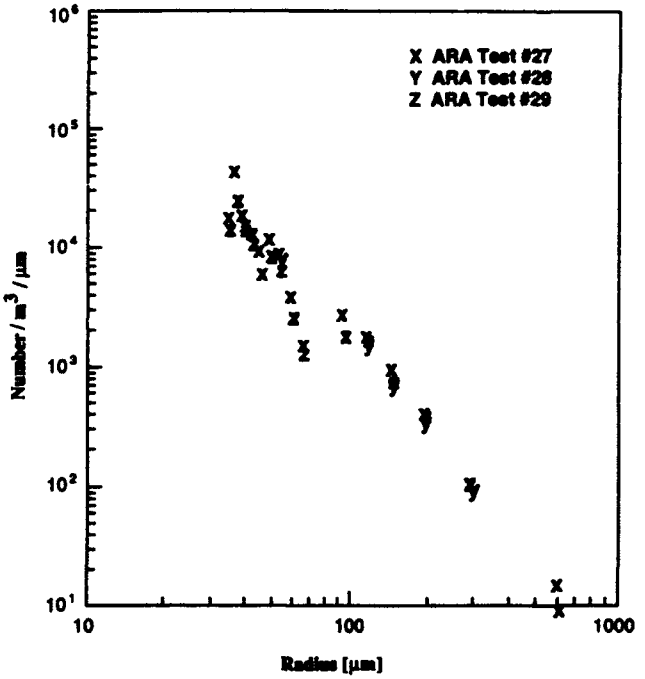

FIG. 16. Three sets of ARA measurements under similar conditions.

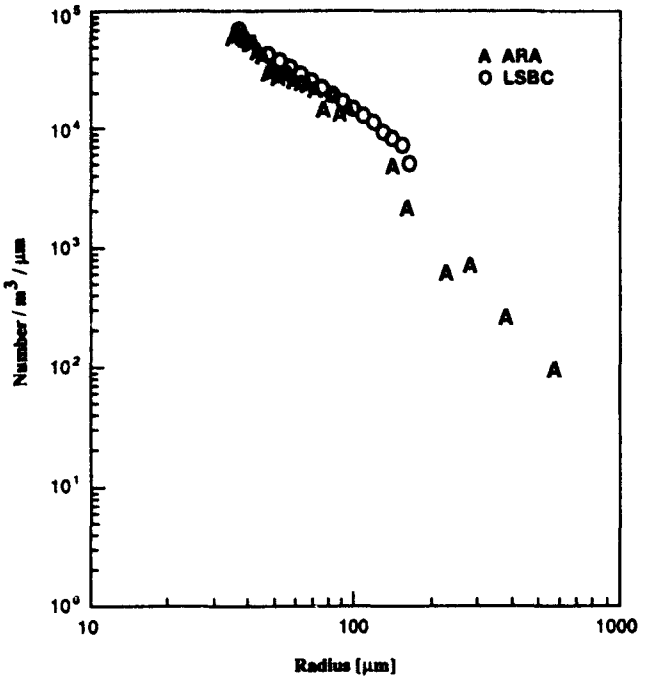

FIG. 17. Comparison of bubble densities generated by water jet, measured by LSBC and ARA.

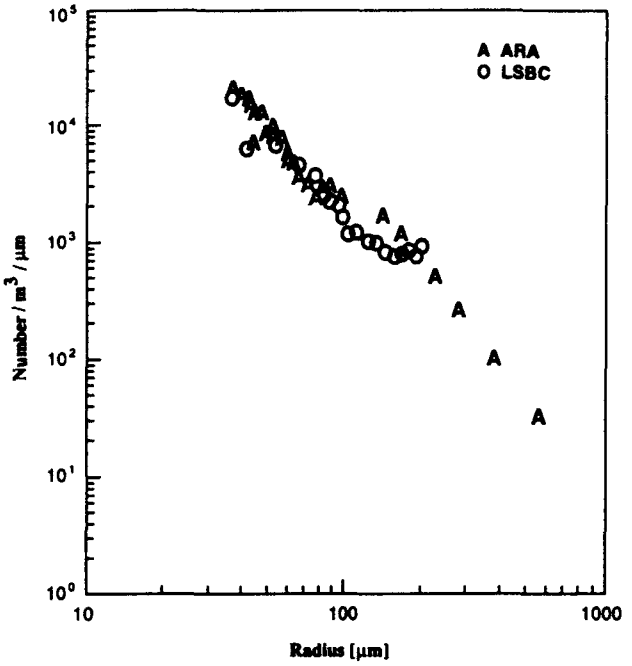

FIG. 19. Comparison of bubble densities generated by water jet, measured by LSBC and ARA.

radii range from 30 to 200 μm, given the condition that bubble plumes are statistically steady and that the measurement time is sufficiently long. These reasons are as follows: First, the bubble density is obtained in the LSBC by a simple counting of individual bubbles in a definite and well-defined sample volume. Second, the determination of the bubble radius for those bubbles are based on the quite accurate terminal velocity relationship with respect to bubble size, confirmed in the laboratory, resulting in a very linear calibration curve. Third, the ARA uses some physical approximations in deriving the inversion formula and has a less well-defined sample volume that is not uniformly active with respect to acoustic extinction and that must contain many bubbles. Taking these factors into consideration, we conclude that the bubble densities measured by the LSBC in its applicable range (30–200 μm) are the most reliable reference data that we have. The very close agreement between the bubble densities shown in Figs. 17–19 by the ARA and LSBC, in effect, proves the nearly equal accuracy of the ARA method, far beyond the more limited supporting evidence originally given by Breitz and Medwin (1989). The smooth and regular extension of the bubble density beyond the $r = 200$ μm in these figures further strongly suggests that the accuracy of the ARA may be taken up to $r = 1200$ μm.

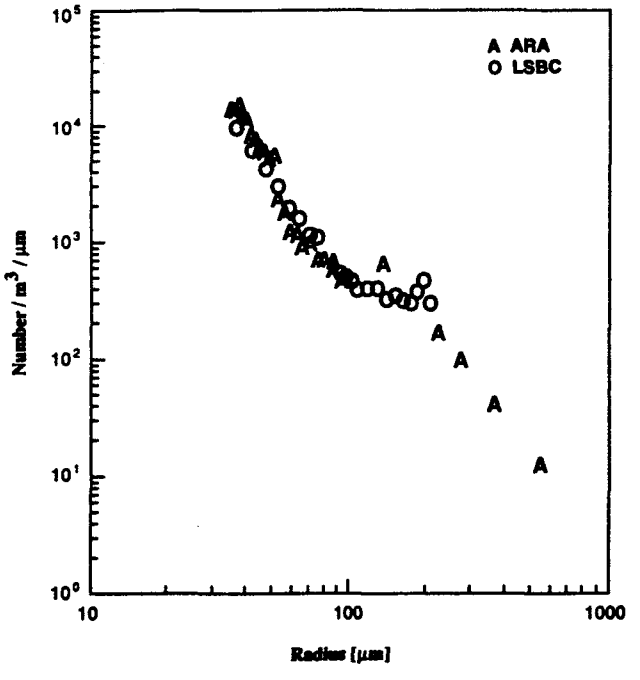

FIG. 18. Comparison of bubble densities generated by water jet, measured by LSBC and ARA.

5. Summary and conclusions

We (NRL and CSS) have jointly conducted two series of laboratory-controlled tests in order to compare the performances of a photographic bubble imaging system (developed at NRL), a light-scattering bubble counter (developed at CSS), and an acoustic resonator

array (developed at NRL). Three kinds of bubble generation methods—electrolysis, hypodermic needle array, and underwater jet air entrainment—were employed to provide bubble plumes in the test tank common to any pair of two bubble sensors under test. We found, however, that the underwater jet air entrainment provided the most suitable bubble plumes for our comparison tests. As such, we presented only the results of using the bubble generation method in this paper. Bubble densities were obtained from all three bubble sensors under the same bubble plumes. Comparisons of these bubble densities shows that over the bubble radius range from about 75 to 400 μm, the results from photographic bubble imaging system agree well with the acoustic resonator array, but that beyond the above range, the former deteriorated rapidly due to photographic film insensitivity and statistical undersampling. This comparison further shows that, over the radius range of 34–200 μm, the light-scattering bubble counter agrees remarkably well with the acoustic resonator array. Since among these three bubble sensors, the acoustic resonator array has the largest sampling volume, fastest response time, and widest radius range (at present from 34 to 1200 μm and can be extended to 8 μm to 2.5 mm) and is the easiest to operate and perform automatic data analyses, it is obviously the most suitable method for bubble density measurements in the oceanic upper layer. As a matter of fact, we have deployed three times, in 1991–92, the NRL's ARA in the oceans for bubble density measurements under moderate to storm conditions (wind speed 10–17 m s^{-1}). Results of these field measurements are being analyzed and are to be published in the near future. The bubble measurement closest to the surface is about 25 cm, the same as reported by Medwin and Breitz (1989). However, in some laboratory situations with more confined test space and steady bubble plumes, the light-scattering bubble counter is unquestionably more suitable.

It is too often that bubble sensors are developed and used without having any comparison with existing sensors under carefully controlled situations. In conducting these comparison tests, both agencies (NRL and CSS) learned valuable lessons concerning the three sensors tested.

Acknowledgments. We would like to thank Raymond Burge, NRL, for assistance in preparing these tests. The portion of this work by NRL is supported by Office of Naval Research Program Element 0601153N, Acoustic Reverberation SRP, Dr. Marshall Orr, program manager. We also thank Dr. A. W. Green for his suggestion for improving an earlier manuscript.

REFERENCES

Breitz, N., and H. Medwin, 1989: Instrumentation for in-situ acoustical measurements of bubble spectra under breaking waves. *J. Acoust. Soc. Am.*, **86**, 739–743.

Commander, K. C., and R. J. McDonald, 1991: Finite-element solution of the inverse problem in bubble swarm acoustics. *J. Acoust. Soc. Am.*, **89**, 592–597.

Henyey, F. S., 1990: Acoustic scattering from ocean microbubble plumes in the 100 Hz to 2 kHz regions. Arete' Associates *ARS-90-023-TR*. [Available from Arete' Associates, P. O. Box 8050, La Jolla, CA, 92038.]

Johnson, B. D., and R. C. Cooke, 1979: Bubble populations and spectra in coastal waters: A photographic approach. *J. Geophys. Res.*, **84**, 3761–3766.

Ling, S. C., and H. P. Pao, 1988: Study of micro-bubbles in the North Sea. *Sea Surface Sound*, B. R. Kerman, Ed., Kluwer Academic Publishers, 197–210.

Medwin, H., and N. D. Breitz, 1989: Ambient and transient bubble spectral densities in quiescent areas and under spilling breakers. *J. Geophys. Res.*, **94**, 12751–12759.

Prosperetti, A., 1988: Bubble related ambient noise in the ocean. *J. Acoust. Soc. Am.*, **84**, 1042–1054.

Su, M. Y., S. C. Ling, and J. Cartmill, 1988: Optical microbubble measurement in the North Sea. *Sea Surface Sound*, B. R. Kerman, Ed., Kluwer Academic Publishers, 211–224.

Walsh, A. L., and P. J. Mulhearn, 1987: Photographic measurements of bubble populations from breaking wind waves at sea. *J. Geophys. Res.*, **92**, 14553–14565.

Wu, J., 1987: Bubbles in the near-surface ocean: A general description. *J. Geophys. Res.*, **93**, 587–590.